



Direct synthesis of acetic acid by simultaneous co-activation of methane and CO₂ over Cu-exchanged ZSM-5 catalysts

Abdelrahman M. Rabie ^{a,b,*}, Mohamed A. Betiha ^b, Sang-Eon Park ^{a,**}

^a Laboratory of Nano-Green Catalysis, Department of Chemistry, Inha University, Incheon, South Korea

^b Egyptian Petroleum Research Institute, Nasr City, Cairo, 11727, Egypt

ARTICLE INFO

Article history:

Received 25 January 2017

Received in revised form 28 April 2017

Accepted 19 May 2017

Available online 22 May 2017

Keywords:

Co-activation of CH₄ and CO₂

Acetic acid

Cu⁺-K-ZSM-5

Continuous catalytic system

ABSTRACT

The ultimate goal of this study is the development of a new strategy to exploit methane and carbon dioxide resources more efficiently and cleanly. Due to the high stabilities of both methane and CO₂, simultaneous C–H bond activation of methane and CO₂ is one of the toughest challenges in catalysis. Formation of acetic acid was achieved under the continuous flow micro-reactor system by the concurrent feed of methane and carbon dioxide over Cu loaded M⁺-ZSM-5 catalysts (M = Li⁺, Na⁺, K⁺ and Ca⁺⁺). The formation of acetic acid was observed in the temperature regime of 425–525 °C with a co-feed of CO₂ and CH₄, under low space velocity of 360 ml h⁻¹ based on methane. Compared to Cu⁰-H-ZSM-5, the M⁺-ZSM-5 catalyst showed remarkable increment in the formation rate of acetic acid, and the catalytic efficiency was in order K > Na > Ca > Li. The obtained results indicated that the M⁺ assists in enriching surface active CO₂ in the form of carbonates and subsequently reacted with the homolytically activated C–H over Cu⁰-H-ZSM-5. Gathering Cu⁰ and M⁺, the Cu⁰-K-ZSM-5 catalyst showed the highest formation rate of acetic acid (395 μ mole gcat⁻¹ h⁻¹) at steady state, for 10 h time-on-stream at 500 °C.

© 2017 Elsevier B.V. All rights reserved.

1. Introduction

Valuable chemicals from abundant resources, which are global warming gasses like CO₂ and methane, evoke great attention not only from the viewpoints of both energy and environmental issues but also due to their potential utilization as an alternative and economic feedstock [1–7]. For the catalytic conversions of methane and CO₂, surface activation using heterogeneous catalyst has been proposed as one of the plausible ways to overcome very high thermodynamic and kinetic stability [8,9]. However, this reaction is thermodynamically very unfavorable (with ΔG° = 16.98 kcal mol⁻¹) [10]. It was assessed that even under extraordinary test conditions (at 725 °C, 100 atm and with CO₂ (95%) and CH₄ (5%)) thermodynamic equilibrium conversion of methane was as low as 1.6 × 10⁻⁶. Moreover, the simultaneous activation of both molecules looks attractive but even tougher [11]. The C–H bond activation of methane has been applied through the non-oxidative or oxidative conditions with the help of oxidants by

catalytic dissociating of C–H bond of methane [12,13]. Nevertheless, the CO₂ activation has been believed to need a reductant to lose oxygen or at least should be activated molecularly with the help of metallic Lewis acid sites or basic sites [14].

With respect to acetic acid, the most prevailed acetic acid manufacturing process is methanol carbonylation process, which has three steps over rhodium and iridium complexes with HI system [15]. Thus, the one-step formation of acetic acid via the carboxylation of methane with CO₂ through the simultaneous activation of these two molecules in the same catalyst system is subjected to have great merits comparing to current major acetic acid processes but very challengeable for simultaneous activation of both reactant molecules due to the high thermodynamic barrier. Acetic acid from CH₄ and CO₂ was firstly reported by Pd/Cu complexes [16] in CF₃COOH solvent, and K₂S₂O₈ (15 mol%) acts as an oxidizing agent homogeneously, which furnished 7% yield on acetic acid. However, it was explained later that no CO₂ participated, but CF₃COOH acted as a carboxylate source due to the more thermodynamically favorable reaction between CH₄ and CF₃COOH. Heterogeneous approaches mostly have adopted the two-step, stepwise, periodic or cyclic reaction modes by using Co-Cu, V₂O₅-PdCl₂/Al₂O₃, Pd & Rh/TiO₂, Pd & Rh/SiO₂, Pd/C and Pt/alumina as catalysts with less than 45 μ mole gcat⁻¹ h⁻¹ of formation rate and poor selectivity as well [17–19]. Huang et al. [20] proposed two-step process for the synthesis of acetic acid over bimetallic Co-Cu catalysts by alterna-

* Corresponding author at: Egyptian Petroleum Research Institute, Petrochemical department, Nasr City, Cairo, 11727, Egypt.

** Corresponding author.

E-mail addresses: abdo3040@yahoo.com (A.M. Rabie), separk@inha.ac.kr (S.-E. Park).

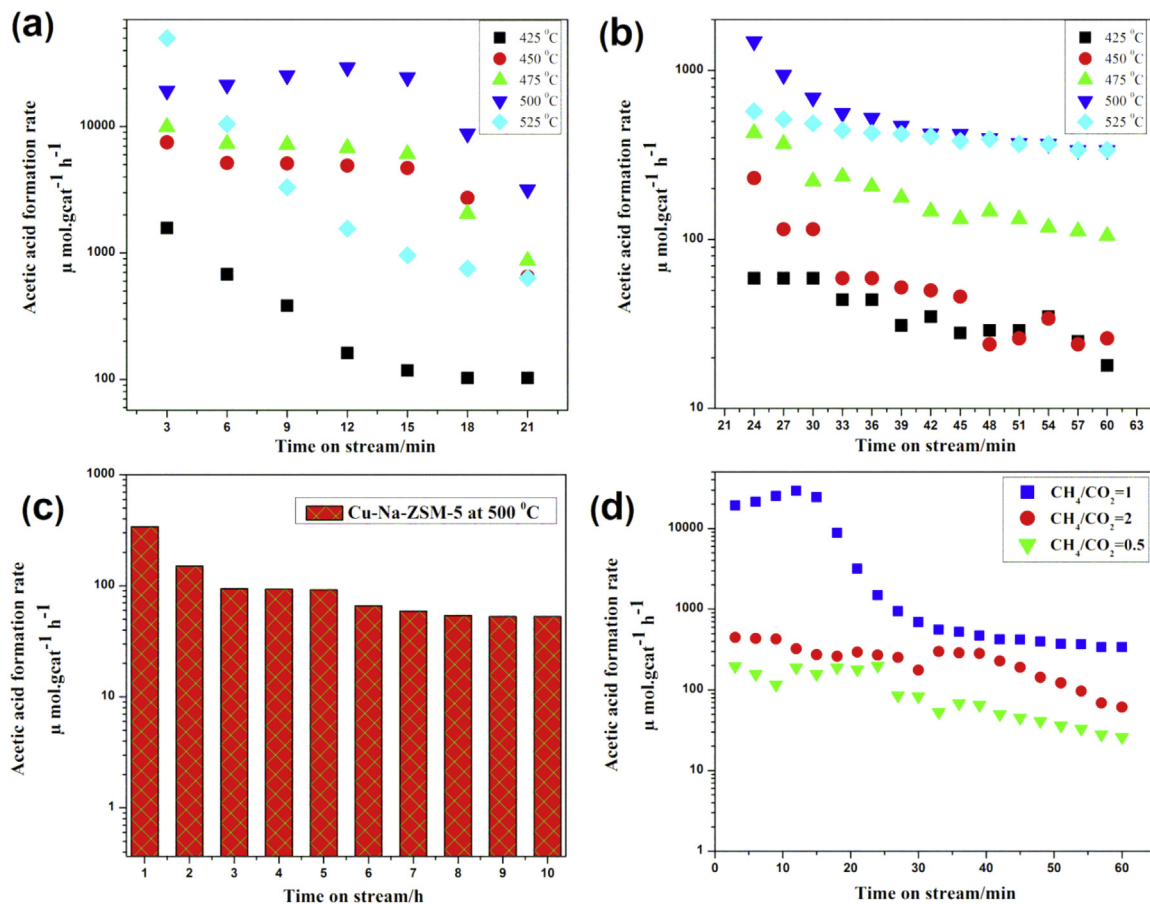


Fig. 1. Acetic acid formation rates on the reaction time over $\text{Cu}^0\text{-Na-ZSM-5}$; initial activities for 21 min (a); and activities from 24 min till 1 h (b) at different temperatures; acetic acid formation rates for 10 h at 500 °C (c); and effect of CH_4/CO_2 flow ratios on the formation of acetic acid at 500 °C (d).

tive feeding of CO_2 and CH_4 with H_2 sweeping between the cycles to give various oxygenates including poor acetic acid selectivity. Wang et al. [21] demonstrated a favorite thermodynamically route of CO^{--} than CO , which could be formed by dielectric-barrier discharge. The direct synthesis of acetic acid from CO_2 is a fascinating reaction. A few authors have prior written about the likelihood to specifically synthesis of acetic acid from CO_2 and CH_4 , especially on metallo-zeolites, regardless of the possibility that basically in view of theoretical studies [22]. For instance, Panjan et al. [9] have explored this reaction from a theoretical approach on an Au-ZSM-5 zeolite. The activation of the C–H bond over the Au-ZSM-5 zeolite would promptly happen through the homolytic σ -bond activation with an energy barrier of 10.5 kcal mol $^{-1}$, and the resulting proton exchange from the Au cation to the zeolitic oxygen, yielding a stable methyl–gold complex adsorbed on the Brønsted acid site of ZSM-5 zeolite. Furthermore expressed that, the transformation of CO_2 on the bi-functional catalyst includes Brønsted acid site assuming a role in the protonation of CO_2 and the methyl–gold complex as a methylating agent. Wu et al. [23] rather examined the formation of acidic acid from CH_4/CO_2 on zinc-changed H-ZSM-5. They demonstrated that zinc site productively activates CH_4 to form zinc-Me species ($-\text{Zn}-\text{CH}_3$) that is additionally subjected to further CO_2 insertion to produce surface acetic acid derivation species (acetate). Also, the Brønsted acid site assumed to play a critical role in the final formation of acidic acid by proton transference to surface acetate species. In both cases, there is a development of a methyl radical intermediate (likely stabilized out by the association with the metal and the zeolitic cage), which then reacts with CO_2 , likely initiated by the interaction with the Brønsted acid sites. Ensuing,

the catalyst used for CO_2 methanation is in charge of changing the chemical structure of reactants that were feed into the reactor.

Zhang et al. [24] studied the conversion of both CH_4 and CO_2 directly to acetic acid by DFT-GGA calculation on Cu (1 1 1) surface and proposed the formation of bi- CH_3COO is kinetically and thermodynamically favored than other predicted pathways and the hydrogenation of bi- CH_3COO species could be achieved through H^+ of Cu (1 1 1) with assistance of the high exothermic reaction of CO_2 and CH_3 molecules. Sangthong et al. [25] studied the direct formation of acetic acid on Au-ZSM-5 catalyst by the DFT (M06-L) and proposed homolytic dissociation of CH_4 on Au cation site, forming stable $\text{CH}_3\text{-Au}$ complex and H-ZSM-5 support protonated CO_2 molecule. Zhu et al. [26] confirmed by FTIR the formation of CH_x and CH_xO species over Cu/Co supported oxide catalysts, and Wu et al. [23] agreed and proved the formation mechanism of M- CH_3 by ^{13}C NMR. Recently, Narsimhan et al. [27] proved the direct conversion of CH_4 and CO_2 onto acetic acid using Cu-exchanged zeolites (ZSM-5 and MOR.) was through the formation of the methoxy-MOR complex. However, to the best of our knowledge, there is no report deals with the experimental study for the direct synthesis of acetic acid from CH_4 and CO_2 under continuous fixed-bed reactor using concurrent feeding. Here we take the next step to perform one-step catalytic conversion of CO_2 and CH_4 to acetic acid using copper exchanged M-ZSM-5 ($M = \text{Li}^+, \text{Na}^+, \text{K}^+$ and Ca^{++}) under for the first time in continues fixed-bed reactor. The beneficial gathering effect of metallic Cu species and the basic cations as a bifunctional catalyst for the simultaneous activation of CH_4 and CO_2 to enable the continuous formation of acetic acid is well discussed.

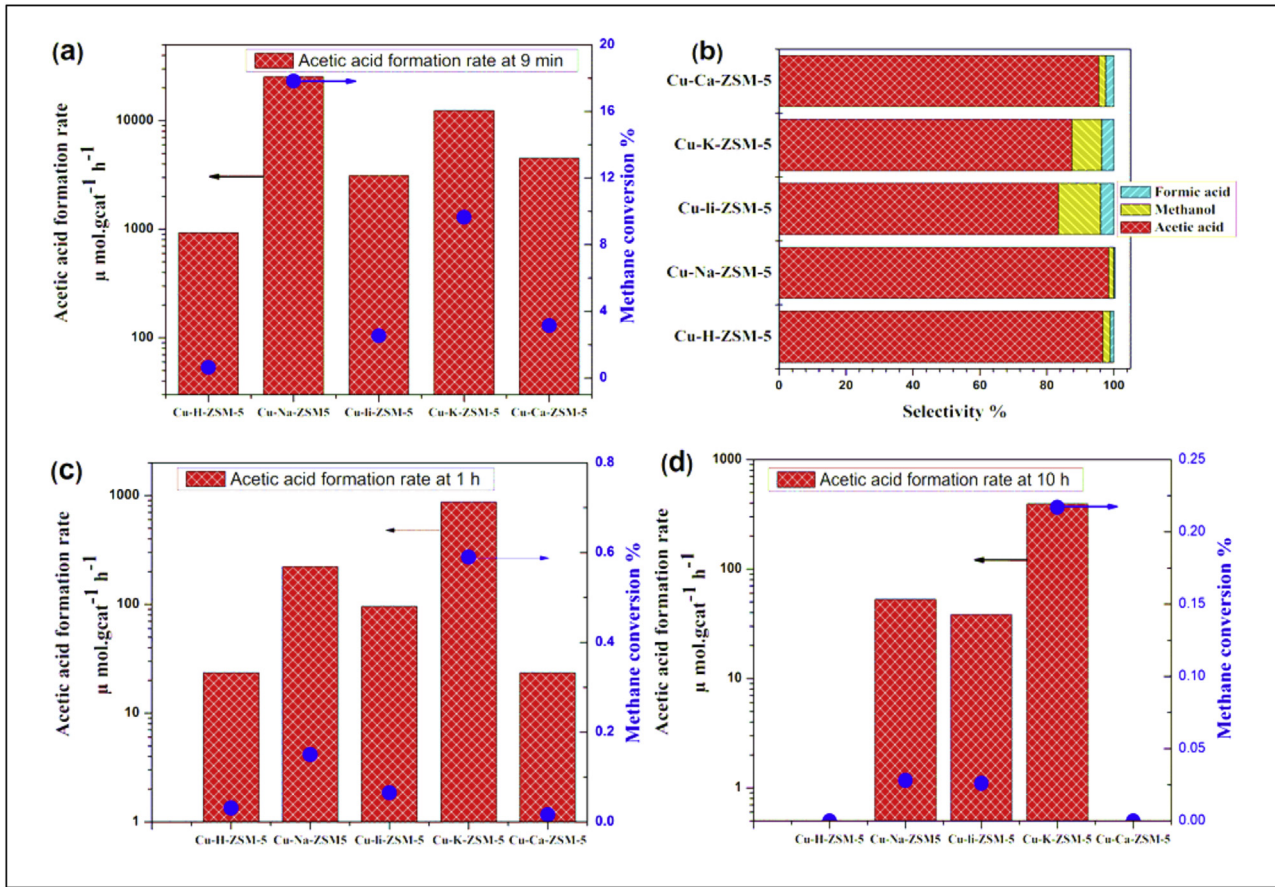


Fig. 2. Methane conversion and acetic acid formation rate over different cation exchanged Cu-M-ZSM-5 catalysts at 500 °C; methane conversion and acetic acid yields (a); and product distribution in liquid products (b); at 9th min of time-on-stream; methane conversions and acetic acid yields at 1 h (c); and after 10 h of time-on-stream (d).

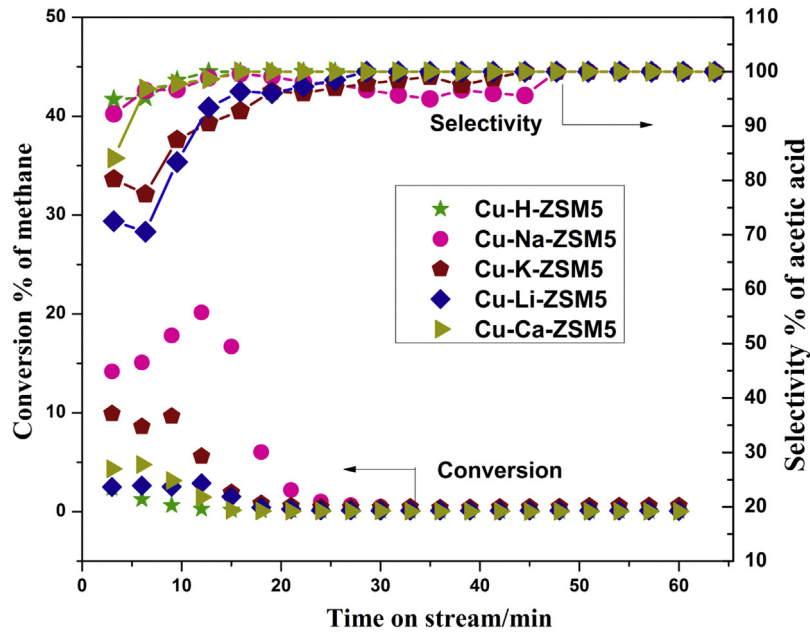


Fig. 3. Methane conversion and acetic acid selectivity over different cations exchanger Cu⁰-M-ZSM5.

2. Experimental

2.1. Preparation of M-ZSM-5

Firstly, the commercial ammonium ZSM-5 is air-calcined at 550 °C for 6 h to form H-ZSM-5. Then, H-ZSM-5 (1.0 g) was sus-

pended three times in fresh 50 ml (0.1 M) NaNO₃ solution for 12 h. The sample was washed thoroughly with hot water/methanol mixture to remove the adsorbed salts. Next to drying at 110 °C, the Na-ZSM-5 was calcined at 500 °C for 5 h. Other samples were pre-

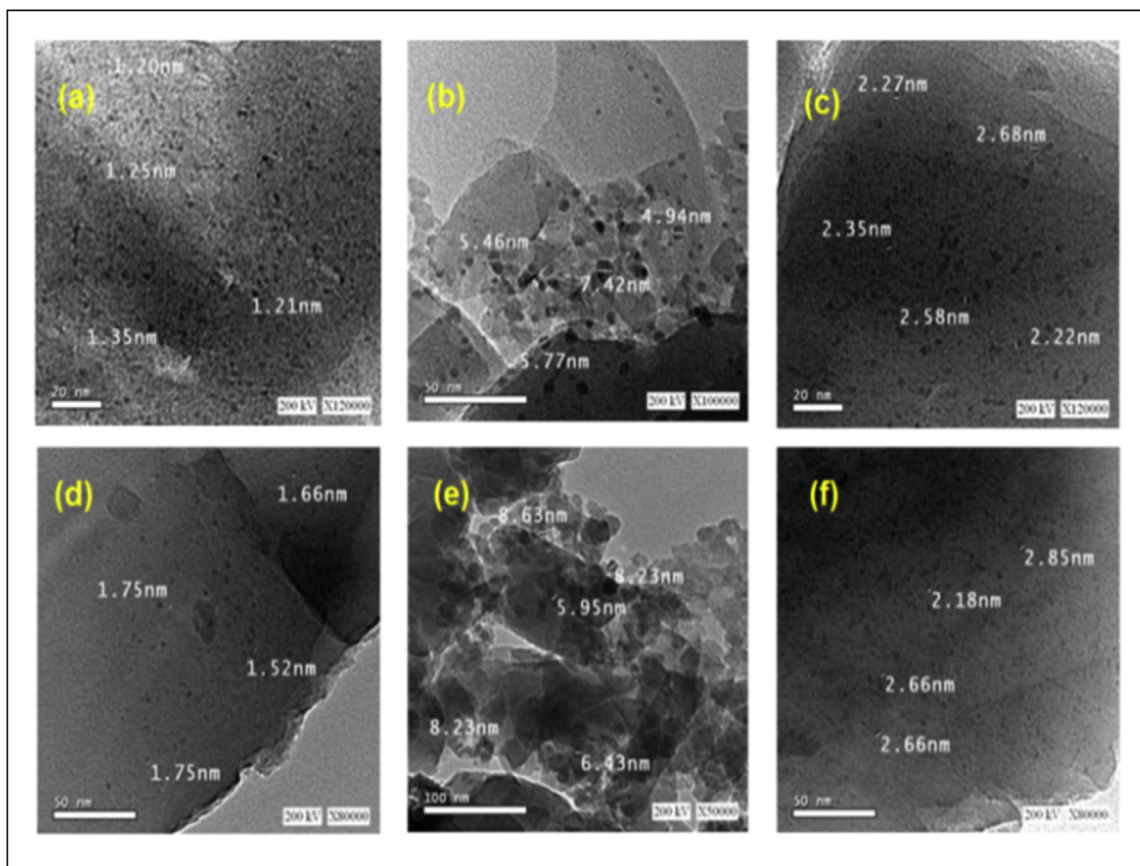


Fig. 4. HR-TEM images of fresh calcined Cu-Na-ZSM5 (a); Used Cu-Na-ZSM5 (b); Regenerated Cu-Na-ZSM5; fresh calcined Cu-K-ZSM5 (d); Used Cu-K-ZSM5 (e); Regenerated Cu-K-ZSM5 (f).

pared following the same route to obtain Li-ZSM-5, K-ZSM-5 and Ca-ZSM-5.

2.2. Preparation of Cu-M-ZSM-5

The copper substituted M-ZSM-5 was carried out by refluxing 1.0 g of M-ZSM-5 in 50 ml of 0.25 M of $\text{Cu}(\text{NO}_3)_2 \cdot 3\text{H}_2\text{O}$ for 6 h. The precipitate was filtered off, washed thoroughly with deionized water, vacuum dried and calcined at 550 °C for 5 h. The copper substituted M as indicated by ICP in ZSM-5 was represented 22.1, 15.6, 20.2 and 16.1%, while the reaming cations were of 0.06, 0.14, 0.16 and 0.25% in Cu-Li-ZSM-5, Cu-Na-ZSM-5, Cu-K-ZSM-5, and Cu-Ca-ZSM-5, respectively. Hence, the molar ratios of Cu/M were 40.57, 40.68, 40.35 and 20.88 for Cu-Li-ZSM-5, Cu-Na-ZSM-5, Cu-K-ZSM-5, and Cu-Ca-ZSM-5, respectively.

2.3. Characterization of the catalysts

The Powder X-ray diffraction patterns (XRD) were obtained using Rigaku Miniflex X-ray diffractometer with $\text{CuK}\alpha$ radiation ($\lambda = 0.154$ nm) at 30 kV and 15 mA from 5° to 90°. The reduced samples were kept in under an inert gas atmosphere and under ambient conditions to avoid the formation of CuO_x . The UV-vis-NIR diffuse reflectance spectra (DRS) were performed with a Shimadzu UV-2501PC spectrophotometer equipped with a reflectance attachment, and BaSO_4 was used as the reference material. The NIR spectra were recorded in the reflectance mode at room temperature. The FTIR spectra were recorded using a Nicolet Impact 410 spectrometer over a range of 400–4000 cm⁻¹. The Brunauer, Emmett, and Teller (BET) surface area of the catalysts was measured using Quanta Chrome AS1Win, Quanta Chrome Instrument v2.01.

Prior to such measurements, all samples were perfectly degassed at 200 °C for 6 h before experiments. The X-ray photoelectron spectra were obtained using an ESCALAB MK II spectrometer provided with a hemispherical electron analyzer and Al anode X-ray exciting source ($\text{AlK}\alpha = 1487.6$ eV). The TEM images of the samples were recorded on a JEOL JEM-2100 (Japan) operating at 200 kV. Temperature-programmed reduction (TPR) of the catalysts with hydrogen (5 vol.% H_2 in helium) was performed from 50 to 600 °C with a heating rate of 10 °C/min in a conventional flow system equipped with a TCD detector for monitoring of the H_2 consumption.

2.4. Catalytic activity

The direct reaction between CH_4 and CO_2 was carried out in stainless fixed-bed reactor loaded with the appropriate amount of catalyst (250 mg). The catalyst was flashed with He-gas (30 ml/min) for 30 min at 120 °C to remove the air and humidity. Subsequently, He gas flow was switched to hydrogen (5 ml/min), and the catalyst was reduced using a temperature program from 30 to 400 °C in 30 min, and the temperature was further raised to 450 °C in 30 min and maintained for 2 h. Then, the desired temperature for the reaction was adjusted under hydrogen flow 2 ml/min. After the reduction, through $x\text{CH}_4$ and CO_2 (1.5 ml/min) that gives a molar ratio of 2, 1 and 0.5, were co-fed simultaneously into the reactor. The reaction was conducted at different temperatures from 425 °C to 525 °C. A reference calcined sample was tested to identify the main active species on the ZSM-5 support. However, the calcined sample showed no catalytic activity toward the acetic acid formation, indicating the prime active species is Cu^0 . The products

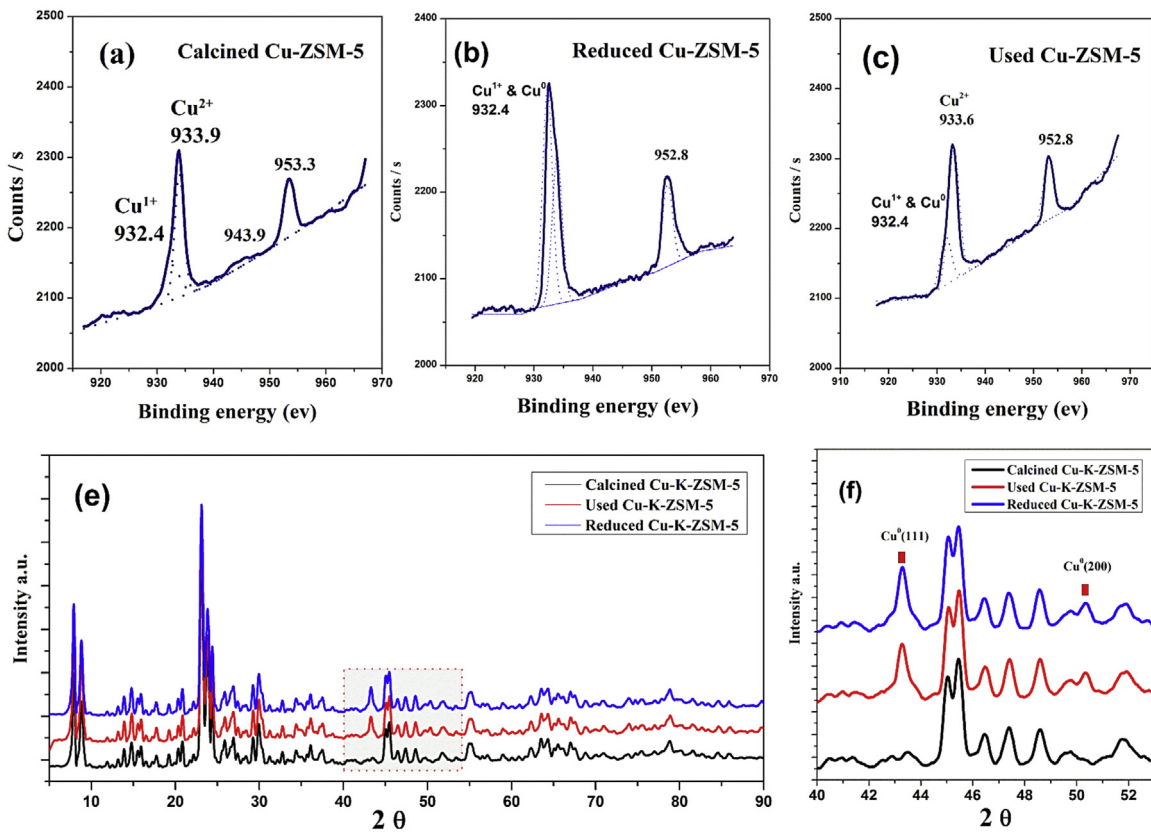


Fig. 5. XPS and XRD results of Cu-ZSM-5: XPS of fresh calcined Cu-ZSM-5 (a); used Cu-ZSM-5 (b); and reduced Cu-ZSM5 (c); XRD of calcined Cu-ZSM-5, reduced Cu-ZSM-5 (e&f).

were analyzed by online gas chromatography (Younglin Instrument, Acme 6000 series, Korea) equipped with FID and TCD.

3. Results and discussion

3.1. Screening the catalytic performance at different temperature and molar ratios of methane and CO₂

Fig. 1 depicts the rates of acetic acid formation depending on temperature; (a) the initial activity within 21 min, (b) till 1 h after 21 min; (c) hourly activities at 500 °C and (d) dependency of CH₄ to CO₂ flow ratios over the Cu⁰-Na-ZSM-5 catalyst. The catalytic activity was tested between 425 and 525 °C. The activities towards the formation of acetic acid increased with temperatures. Interestingly steady formation of acetic acid was observed with the highest at 500 °C for 10 h of time-on-stream. Since acetic acid formation is directly dependent on the flow ratios of methane and CO₂, thus the flow optimization was carried out as shown in **Fig. 1d** and the equimolar flow ratio 1:1 of methane and CO₂ showed the highest rate of formation of acetic acid at 500 °C.

3.2. Effect of basic cations

In order to know the role of basic cations (M=Li⁺, Na⁺, K⁺ and Ca⁺⁺) in Cu⁰-M-ZSM-5 catalysts, their activities were compared to Cu⁰-H-ZSM-5 catalyst (**Fig. 2**) at the initial 9th min (**Fig. 2a**), 1 h (**Fig. 2c**) and 10 h (**Fig. 2d**) time-on-stream. **Fig. 2b** showed the product distributions that gave formic acid, methanol, and acetic acid at the initial period of 9th min, while after 1 h, the acetic acid had a selectivity of ~100%. For the whole range of reaction temperatures, Cu⁰-H-ZSM-5 catalyst gave poor conversion than any other basic cation exchanged Cu⁰-M-ZSM-5 catalysts. Cu-K-ZSM-

5 catalyst gave the highest activity (395 μ mol.g⁻¹ h⁻¹) after 10. This indicates that the activation of CO₂ is closely related to the alkali cations, which helps to insert onto C–H activated species from methane. The higher CO₂ adsorption capacity in Cu-K-ZSM5 is attributed to the acid-base interaction between the ZSM-5 framework and CO₂ molecules. Even the Cu-Na-ZSM-5 catalyst gave the highest formation rate at the initial period but showed a more drastic decline after 1 h than Cu-K-ZSM-5 (**Fig. 2c**). It is reported that the CO₂ adsorption capacity slightly increases with the cation size as follow Li < Na < K, however, the population of divalent cation at the pore entrance of zeolite framework is less and has an only half number of cation than that of monovalent exchanged ZSM-5, which explains the low activity in Ca-exchanged ZSM-5 catalyst [28]. The CO₂-TPD of the Cu-K-ZSM-5 catalysts exhibited the highest concentration of adsorbed CO₂ among all of the prepared catalysts (**Fig. S1.†**). So, the effective charge density of the cations inside the zeolite pores is the reason for higher CO₂ adsorption. The experimental results were observed to match reasonably with the above explanation.

3.3. Effect of catalyst regeneration

The regeneration studies were performed in the cases of Cu-K-ZSM-5 and Cu-Na-ZSM-5 catalysts. The used catalysts after 10 h of reaction were air-calcined at 550 °C for 5 h in the muffle furnace and tested after reduction according to item 2.4 for another 10 h as shown in (**Table S1.†**). The regenerated catalysts showed comparable activities to those of fresh catalysts (~70% regarding formation rate of acetic acid). The activities of both fresh and regenerated catalysts (**Fig. S2.†**), are showed a steady decline in the catalytic activity. **Fig. 3** shows plots of the methane conversions and acetic acid selectivity over Cu-M-ZSM-5 catalysts. Methane conversion decreased

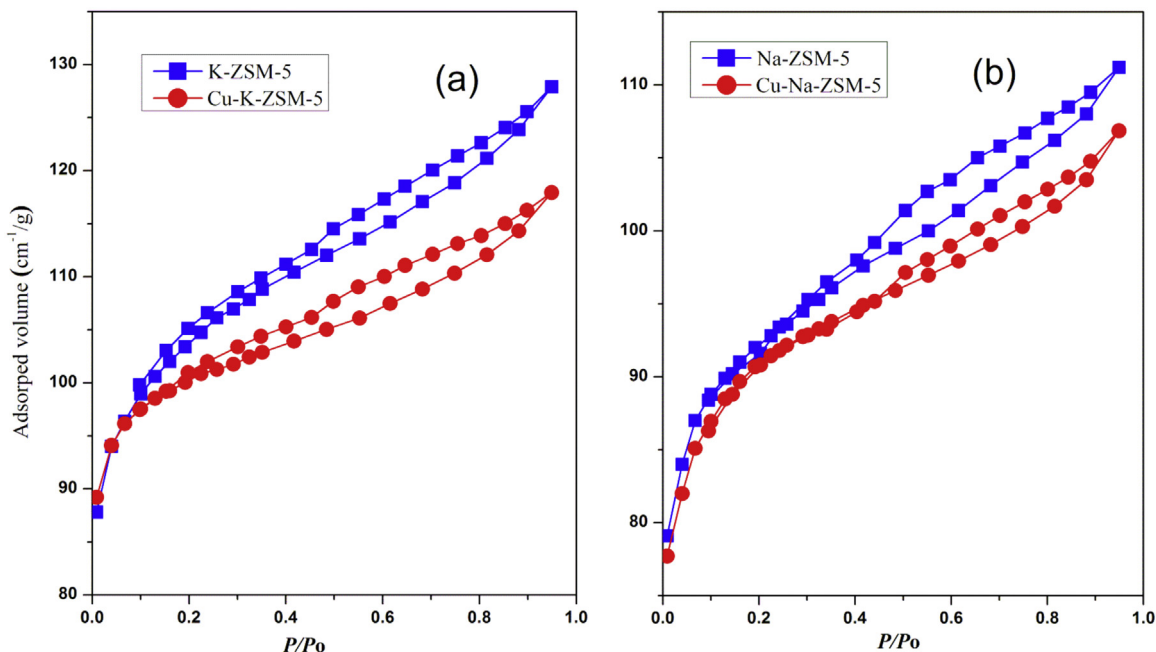


Fig. 6. N₂-adsorption-desorption isotherms of (a) Na-ZSM-5 and Cu-Na-ZSM-5; (b) K-ZSM-5 and Cu-K-ZSM-5.

significantly for all of the catalysts after 21 min, may be due to the aggregation of the Cu⁰ nanoparticles or due to the carbon formation with each elementary of CH₃-H activation, which has high barrier energy (> 190 kJ/mol) [29]. Varghese et al. [29] reported that the metal aggregation increased their corresponding free energy barriers due to the difficult reorganization of deposited copper species to accommodate CH₃-H.

More profound evidence on the catalyst deactivation and regeneration, the fresh calcined, used and regenerated catalysts were obtained by TEM as shown in Fig. 4. The TEM micrograph of the synthesized Cu-K-ZSM-5 and Cu-Na-ZSM-5 revealed the formation of the small size of Cu nanoparticles in the range of 1~2 nm and had a good dispersion on ZSM-5. However, after the reaction, the TEM image reveals the formation of small Cu aggregates with different size in the range of 4~9 nm. This behavior indicates that the Cu nanoparticles are aggregated, resulting in the loss of catalytic activity. The used catalyst was regenerated by calcining in air at 550 °C, which shows the re-dispersion of the aggregated Cu particles size into the smaller size of 2~3 nm again. The particle sizes of the catalysts are comparable with the histogram (Fig. S4.†)

The high-resolution XPS of calcined Cu-K-ZSM-5 catalyst exhibited peaks 933.9 and 953.3 eV that could be attributed to Cu 2p_{3/2} and Cu 2p_{1/2}, respectively, with a gap between two peaks of 20 eV, which is in good agreement with stander CuO value. The presence of shake-up peak at 943.9 eV is attributed to open 3d⁹ shells, which gave evidence for the presence of Cu⁺ state as shown in Fig. 5a. However, it is clear that the value of Cu 2p_{3/2} and Cu 2p_{1/2} is lower than the reported binding energy of CuO [30], suggesting that the Cu species form strong interaction with ZSM-5 support. XPS of the reduced Cu-K-ZSM-5 in Fig. 5b also showed Cu 2p_{3/2} curve-fitted at 932.4 eV, assuming that the reduced catalyst was rich in Cu⁰ species. Also, XPS of the used Cu-K-ZSM-5 in Fig. 5c catalyst showed weak shoulder at 932.4 eV and intense peak at 933.6 eV companies with the absence of collected satellite peak at 943 eV, indicating the presence of both Cu⁰ and Cu¹⁺ species.

XRD analysis was carried out on the three catalysts: calcined, reduced and used Cu-K-ZSM-5. XRD shows the typical diffraction peaks at 2&z.Theta; = 7.94°, 8.85°, 14.90°, 23.33°, 23.90° and 24.50°, which are characteristic to the parent ZSM-5 [31]. Fig. 5f

shows the XRD patterns of the fresh, reduced and used catalyst. The reduced catalyst showed the existence of Cu⁰ species confirmed at 2&z.Theta; = 43° and 51°, which corresponds to the lattice planes of the cubic copper phase (1 1 1) and (2 0 0), respectively [32]. These peaks were also observed in the case of used catalyst.

Fig. 6 shows the N₂-physisorption isotherms and pore size distribution of zeolites. The N₂-take-up at low P/P₀ affirms the presence of micropores, while the N₂ was further uptake till P/P₀ of 5. Regularly, the Na-ZSM-5, K-ZSM-5, Cu-Na-ZSM-5 and Cu-K-ZSM-5 zeolites demonstrate a progressive N₂-take-up over the P/P₀ range and a significant uptake over P/P₀ of 0.4–0.9 with an H4 hysteresis loop, which is characteristic of mesoporous materials. The Pore size distribution data exhibit that the ZSM-5 zeolites contain a lot of mesopores with the size of 3.4 nm that slightly decreases after Cu⁰ loading. For all ZSM-5 zeolites, the pore volume is small. Normalized surface zones (NS_{BET}) gives knowledge into the location of metal species or ascertain out a blockage effect of the guest metal on ZSM-5 materials. The NS_{BET} formula is expressed as [35,36].

$$NS_{BET} = \frac{SA_1}{1-y} \times \frac{1}{SA_2}$$

Where SA_c is the surface area of copper-loaded ZSM-5, SA_s is the surface area of ZSM-5 and y is the mass fraction of copper. When the calculation of the NS_{BET} for Cu-Na-ZSM-5 is close to 1, suggesting the Cu⁰ particles is very fine and located through both internal pores and the external surface. When the NS_{BET} is ≪ 1, suggesting the Cu⁰ particles are blocking the ZSM-5 pore and located on the external surface. The calculation indicates that the NS_{BET} was of 0.98 and 0.96 for Cu-Na-ZSM-5 Cu-K-ZSM-5 zeolites, respectively, suggesting the presence of Cu⁰ in interior and exterior pores as shown in table S3.

EPR and UV-vis-NIR spectra of the calcined Cu-K-ZSM-5 catalyst are telling the presence of the isolated Cu²⁺ ions with tetragonally distorted octahedral coordination. In EPR spectrum, typical Cu²⁺ ion species having axial anisotropy of g factors with parameters g_{||} = 2.33, A = 137 G, g_⊥ = 2.054 (Fig. 7a) and large absorption band in the range of 500–1400 nm centered at 800 nm was observed in (Fig. S3.†). The broad transition band at ca. 600~850 nm in UV, which corresponds to d-d transition ²T_{2g} ← ²E_g, which is inher-

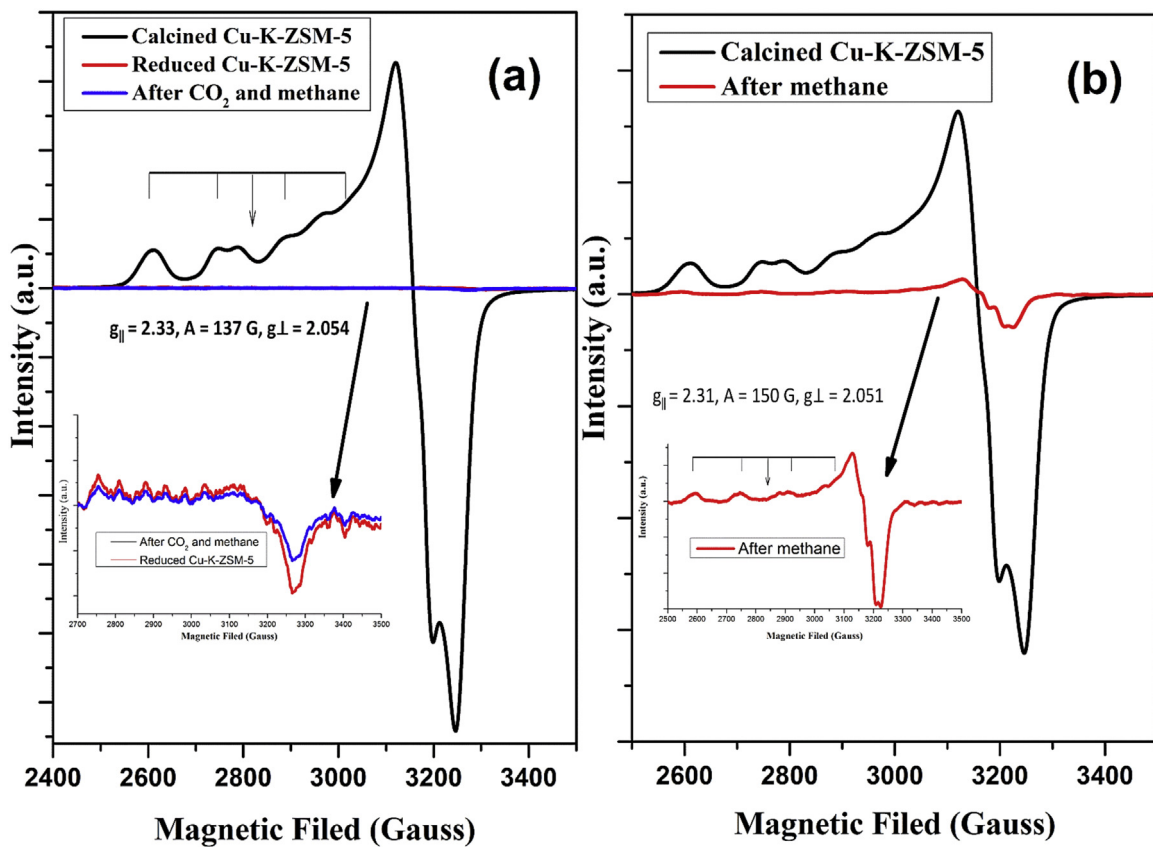


Fig. 7. In-situ EPR of calcined, reduced, and after introducing of methane and CO₂ over Cu-K-ZSM-5 (a); calcined and methane intrusion at 450 °C onto the calcined Cu-K-ZSM-5 (b).

ent of Cu²⁺ ions in zeolites [33]. An intense peak at 250 nm can be assigned to the O²⁻ → Cu²⁺ charge transfer transition. Moreover, the additional peak closed to 365 nm was observed, which is related to d-d transitions of Cu (II) species. The spectrum of these conditions is in agreement with the reported in the literature for comparative specimens and relates to Cu (II) in zeolitic cavities [34].

As shown in the EPR (Fig. 7b) spectroscopy, the adsorption of methane over calcined catalysts have comparably small amounts of isolated Cu²⁺ O_h ions. The EPR spectrum is having axial anisotropy of g factors with parameters $g_{\parallel} = 2.31$, $A = 150$ G, $g_{\perp} = 2.051$. EPR signal intensity shows that the amounts of isolated copper ions Cu²⁺ O_h decreased with methane adsorption, which means the methane reduces Cu²⁺ species to Cu¹⁺ and Cu⁰ by the hydrogen species which were induced through the dissociative activation of methane. This is also reflected in the case of UV-vis DR after adsorption of methane. When the calcined sample was reduced with hydrogen at 450 °C, the "d-d" transitions of Cu²⁺ ions in the range of 500–1400 nm was not observed on the spectrum, as a result of the reduction of Cu²⁺ ions. The H₂ treated Cu-K-ZSM-5 exhibited different line shapes at 230, 314, and 560 nm. The first band showed at 230 nm is corresponding to Cu¹⁺, and second at 314 nm upon reduction at 450 °C is assigned to the internally allowed transition $3d^{10}4s \rightarrow 3d^{10}4f$ of isolated copper atoms of Cu⁰, while the third band at 560 nm in the reduced catalyst is assigned to Cu⁰ and this peak was also observed to be increased after introducing CH₄/CO₂ [37] due to the aggregation of Cu⁰ [38]. These results are in good agreement with EPR analysis, in which a drastic decrease in the intensity of the hyperfine splitting of Cu²⁺ was observed by the intrusion of methane over the calcined Cu-K-ZSM-5 catalyst.

In-situ FT-IR studies were carried out to elucidate the reaction mechanism over Cu-K-ZSM-5 catalyst. Begging, the catalyst was

dosed with H₂ several times, using the same program used for the reduction mentioned in the experimental part to obtain the reduced form of Cu/K⁺-ZSM-5 catalyst. After complete reduction, the catalyst was exposed to a pulse injection of methane and carbon dioxide simultaneously. FT-IR (Fig. 8) showed a peak at 1025 cm⁻¹ attributed to the formation of M-O-CO₂ as a result of activation of CO₂ over M⁺ bonded to ZSM-5 [39]. Nevertheless, the appearance of the peak at 2922 cm⁻¹ is due to the formation of activated methane, Cu...H-CH₃. The peak at 1742 cm⁻¹ can be attributed to the C=O stretch of acetic acid monomer [40], and the additional peak at 1420 cm⁻¹ confirms the existence of O-H deformation in a dimer of acetic acid [41]. The peak at 1660 cm⁻¹ indicates the formation of acetate group ($\nu_{\text{as}}(\text{COO}^-)$). Furthermore, the low-intensity peaks, which are situated near 2960 and 2854 cm⁻¹ and the presence of absorption other than the stretching position of the water-OH group at 3390 cm⁻¹ must be attributed to the carboxyl-OH stretching vibration. The additional peaks corresponding to CO₂ at 2360 and 2340 cm⁻¹ were also observed [41]. According to the data of FTIR, a plausible mechanism towards the formation of acetic acid through co-activation of CH₄ and CO₂ on Cu/K⁺-ZSM-5 zeolite is represented in (Scheme 1). In the initial step, CH₄ activation on Cu/K⁺-ZSM-5 zeolite creates surface a (-Cu-CH₃) species (Step 1). Simultaneously, CO₂ was activated on M⁺-ZSM-5 zeolite that helps in the formation of surface carbonate species where the basic cations help in surface CO₂ adsorption (Step 2). These carbonate species acts like a reservoir which in turn promotes insertion into Cu-CH₃ bond of copper methyl species. These activated surface species transforms into giving a surface acetate intermediate (-Cu-OOC-CH₃) (Step 3). Which then abstracts a proton from the dissociative cleavage of methane and finally the acetic acid product is desorbed from the surface recovering the active site for the con-

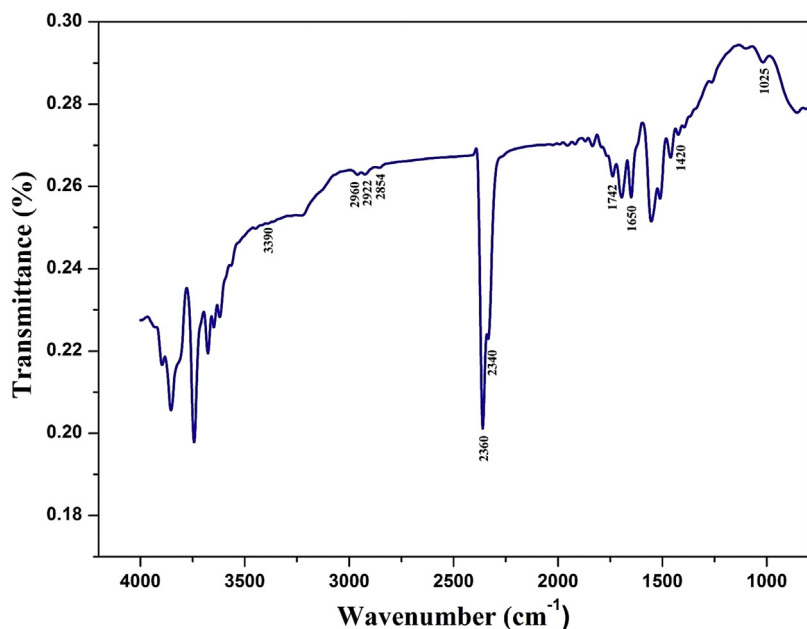
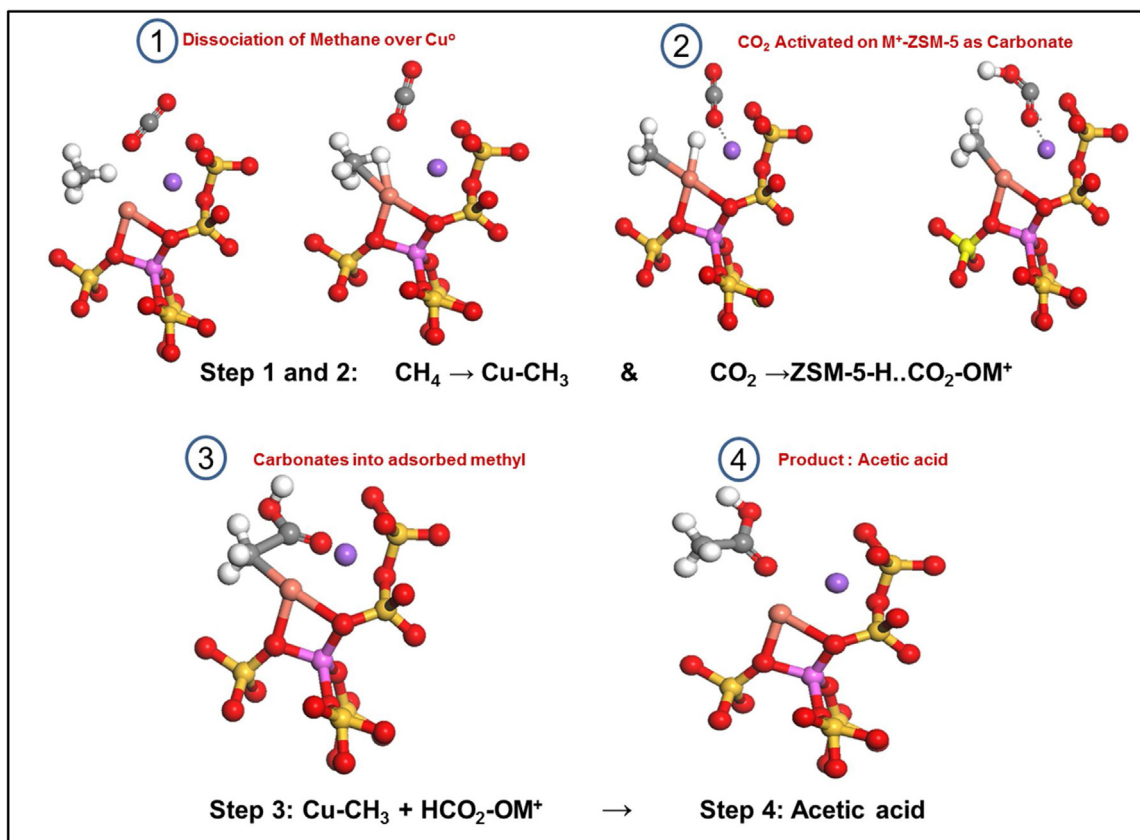


Fig. 8. In-situ IR spectra for Cu-K-ZSM-5 at 450 °C. The catalyst reduced with hydrogen from room temperature to 450 °C then methane and CO₂ introduced simultaneously for 15 min at the same temperature then the IR measured at room temperature.



Scheme 1. An ostensible mechanism for the Co-Conversion of CH₄ and CO₂ into acetic acid over Cu-M⁺-ZSM-5 Zeolite: (Steps 1–3) activation of CH₄ leads to the formation of ($-\text{Cu}-\text{CH}_3$), while the activation of CO₂ helps in the formation of surface carbonate species over cations site. (Steps 4–5): insertion of CO₂ into the ($-\text{Cu}-\text{CH}_3$), produces surface acetate species ($-\text{Cu}-\text{OOCCH}_3$) as a reaction intermediate which abstracts the proton to form acetic acid.

tinuation of the catalytic cycle (Step 4). The proton transfer step is the vital step in the acetic acid synthesis. The Cu-exchanged zeolite helps in stabilizing these protons.

The simultaneous activation of CH₄ and CO₂ is of great significance as both contributes towards global warming and can be converted into fuels which are of particular interest in the chemical industry. The C–H activation over transition metals with fcc(111)

or *hcp*(0001) surfaces is reported by Gong et al., where he collected some of the reaction energies calculated previously which, hinders methane decomposition [42]. To the best of our knowledge, this is the first report where the continuous formation of acetic acid has been demonstrated experimentally using a unique bifunctional zeolite catalyst. The near-perfect selectivity of acetic acid at equilibrium conditions is attributed to the Cu-exchanged zeolite catalyst which was found to be capable of simultaneous activation of methane and to further the reaction of CO₂ with such a prior-activated intermediate on a Cu-exchanged ZSM-5 zeolite to produce acetic acid.

4. Conclusions

In summary, we have developed a new direct method for synthesis of acetic acid by co-activation of methane and carbon dioxide in the one-step process. Cu nanoparticle loaded basic cation ZSM-5 catalysts were proven to activate both methane and carbon dioxide simultaneously in concurrent feed, which enabled to the formation of acetic acid in a continuous flow reactor. The activation of CO₂ was observed to be closely related to the alkali cation in the MFI structure. The formation rate of acetic acid was observed to be in the following order with respect to the cationic species K > Na > Ca > Li, this indicates that basic cation contributes to the activated CO₂ on the surface and thus resulted in high insertion activity. The Cu-M⁺-ZSM-5 catalyst exhibited high starting activity which decreased within an hour but sustained a state-state yield of acetic acid of 395 μ mole gcat⁻¹ h⁻¹ for 10 h. The deactivation was caused mainly due to the aggregation of Cu⁰ species. Upon calcination, the catalyst activity was recovered up to more than 70% which was mainly due to re-dispersion of Cu nanoparticle over the catalyst surface.

Acknowledgements

The financial support for the present work was provided by the National Research Foundation of Korea, Grant funded by the Korean government (NRF-2015K2A4A1036415).

Appendix A. Supplementary data

Supplementary data associated with this article can be found, in the online version, at <http://dx.doi.org/10.1016/j.apcatb.2017.05.053>.

References

- [1] J.J. Carey, M. Nolan, Dissociative adsorption of methane on the Cu and Zn doped (111) surface of CeO₂, *Appl. Catal. B: Environ.* 197 (2016) 324–336.
- [2] P. Gélin, M. Primet, Complete oxidation of methane at low temperature over noble metal based catalysts: a review, *Appl. Catal. B: Environ.* 39 (2002) 1–37.
- [3] M.B. Ansari, B.-H. Min, Y.-H. Mo, S.-E. Park, CO₂ activation and promotional effect in the oxidation of cyclic olefins over mesoporous carbon nitrides, *Green Chem.* 13 (2011) 1416–1421.
- [4] J.-S. Chang, V.P. Vislovskiy, M.-S. Park, J.S. Yoo, S.-E. Park, Utilization of carbon dioxide as soft oxidant in the dehydrogenation of ethylbenzene over supported vanadium–antimony oxide catalysts, *Green Chem.* 5 (2003) 587–590.
- [5] P. Tang, Q. Zhu, Z. Wu, D. Ma, Methane activation: the past and future, *Energy Environ. Sci.* 7 (2014) 2580–2591.
- [6] M. Ovcharov, N. Shcherban, S. Filonenko, A. Mishura, M. Skoryk, V. Shvalagin, V. Granchak, Hard template synthesis of porous carbon nitride materials with improved efficiency for photocatalytic CO₂ utilization, *Mater. Sci. Eng.: B* 202 (2015) 1–7.
- [7] A. Raza, R. Rezaee, C.H. Bing, R. Gholami, M.A. Hamid, R. Nagarajan, Carbon dioxide storage in subsurface geologic medium: a review on capillary trapping mechanism, *Egypt. J. Pet.* 25 (2016) 367–373.
- [8] M.L. Lejkowski, R. Lindner, T. Kageyama, G.É. Bódizs, P.N. Plessow, I.B. Müller, A. Schäfer, F. Rominger, P. Hofmann, C. Futter, The first catalytic synthesis of an acrylate from CO₂ and an alkene—a rational approach, *Chem.– Eur. J.* 18 (2012) 14017–14025.
- [9] W. Panjan, J. Sirijaraensre, C. Warakulwit, P. Pantu, J. Limtrakul, The conversion of CO₂ and CH₄ to acetic acid over the Au-exchanged ZSM-5 catalyst: a density functional theory study, *Phys. Chem. Chem. Phys.* 14 (2012) 16588–16594.
- [10] E.M. Wilcox, M.R. Gogate, J.J. Spivey, G.W. Roberts, Direct synthesis of acetic acid from methane and carbon dioxide, *Stud. Surf. Sci. Catal.* 136 (2001) 259–264.
- [11] J.A. Labinger, J.E. Bercaw, Understanding and exploiting CH bond activation, *Nature* 417 (2002) 507–514.
- [12] B. Arndsten, R. Bergman, The selective intermolecular carbon–Hydrogen bond activations by synthetic metal-complexes in homogeneous solution Mobley, *Acc. Chem. Res.* 28 (1995) 154–162.
- [13] D. Dissanayake, J. Lunsford, M. Rosyne, Site differentiation in homolytic vs. heterolytic activation of methane over Ba/MgO catalysts, *J. Catal.* 146 (1994) 613–615.
- [14] M.B. Ansari, S.-E. Park, Carbon dioxide utilization as a soft oxidant and promoter in catalysis, *Energy Environ. Sci.* 5 (2012) 9419–9437.
- [15] P. Otero-Schipper, W. Wachter, J. Butt, R. Burwell, J. Cohen, I.I.I. PtSiO₂: Activity and selectivity for some hydrogenation reactions, *J. Catal.* 50 (1977) 494–507.
- [16] M. Zerella, S. Mukhopadhyay, A.T. Bell, Synthesis of mixed acid anhydrides from methane and carbon dioxide in acid solvents, *Org. Lett.* 5 (2003) 3193–3196.
- [17] W. Huang, C. Zhang, L. Yin, K. Xie, Direct synthesis of acetic acid from CH₄ and CO₂ in the presence of O₂ over a V2O5-PdCl₂/Al₂O₃ catalyst, *J. Nat. Gas Chem.* 13 (2004) 113–115.
- [18] Y.-H. Ding, W. Huang, Y.-G. Wang, Direct synthesis of acetic acid from CH₄ and CO₂ by a step-wise route over Pd/SiO₂ and Rh/SiO₂ catalysts, *Fuel Process. Technol.* 88 (2007) 319–324.
- [19] E.M. Wilcox, G.W. Roberts, J.J. Spivey, Direct catalytic formation of acetic acid from CO₂ and methane, *Catal. Today* 88 (2003) 83–90.
- [20] W. Huang, Studies on direct of CH₄ and CO₂ to acetic acid by two-step reaction sequence, PhD Dissertation, Taiyuan Univ. Technol. Taiyuan (2003) 65–70.
- [21] J.-g. Wang, C.-j. Liu, Y.-p. Zhang, B. Eliasson, A DFT study of synthesis of acetic acid from methane and carbon dioxide, *Chem. Phys. Lett.* 368 (2003) 313–318.
- [22] S. Abate, K. Barbera, E. Giglio, F. Deorsola, S. Bensaid, S. Perathoner, R. Pirone, G. Cinti, Synthesis, characterization, and activity pattern of Ni-Al hydrotalcite catalysts in CO₂ methanation, *Ind. Eng. Chem. Res.* 55 (2016) 8299–8308.
- [23] J.-F. Wu, S.-M. Yu, W.D. Wang, Y.-X. Fan, S. Bai, C.-W. Zhang, Q. Gao, J. Huang, W. Wang, Mechanistic insight into the formation of acetic acid from the direct conversion of methane and carbon dioxide on zinc-modified H-ZSM-5 zeolite, *J. Am. Chem. Soc.* 135 (2013) 13567–13573.
- [24] R. Zhang, L. Song, H. Liu, B. Wang, The interaction mechanism of CO₂ with CH₃ and H on Cu (111) surface in synthesis of acetic acid from CH₄/CO₂: A DFT study, *Appl. Catal. A: Gen.* 443 (2012) 50–58.
- [25] W. Sangthong, M. Probst, J. Limtrakul, Conversion of CO₂ and C₂H₆ to propanoic acid over a Au-Exchanged MCM-22 zeolite, *ChemPhysChem* 15 (2014) 514–520.
- [26] W. Huang, K.-C. Xie, J.-P. Wang, Z.-H. Gao, L.-H. Yin, Q.-M. Zhu, Possibility of direct conversion of CH₄ and CO₂ to high-value products, *J. Catal.* 201 (2001) 100–104.
- [27] K. Narasimhan, V.K. Michaelis, G. Mathies, W.R. Gunther, R.G. Griffin, Y. Romaín-Leshkov, Methane to acetic acid over Cu-exchanged zeolites: mechanistic insights from a site-specific carbonylation reaction, *J. Am. Chem. Soc.* 137 (2015) 1825–1832.
- [28] R.S. Pillai, E. Titus, CO₂ and N₂ adsorption in nano-porous BEA type zeolite with different cations, *Mater. Today: Proc.* 2 (2015) 446–455.
- [29] J.J. Varghese, S.H. Mushrif, First-principles investigation of the dissociation and coupling of methane on small copper clusters: interplay of collision dynamics and geometric and electronic effects, *J. Chem. Phys.* 142 (2015) 184308.
- [30] Y. Li, T. Sasaki, Y. Shimizu, N. Koshizaki, A hierarchically ordered TiO₂ hemispherical particle array with hexagonal-Non-Close-Packed tops: synthesis and stable superhydrophilicity without UV irradiation, *Small* 4 (2008) 2286–2291.
- [31] J. Liu, W. Song, C. Xu, J. Liu, Z. Zhao, Y. Wei, A. Duan, G. Jiang, The selective catalytic reduction of NO_x over a Cu/ZSM-5/SAPO-34 composite catalyst, *RSC Adv.* 5 (2015) 104923–104931.
- [32] A. Rittermeier, S. Miao, M.K. Schröter, X. Zhang, M.W. van den Berg, S. Kundu, Y. Wang, S. Schimpf, E. Löffler, R.A. Fischer, The formation of colloidal copper nanoparticles stabilized by zinc stearate: one-pot single-step synthesis and characterization of the core–shell particles, *Phys. Chem. Chem. Phys.* 11 (2009) 8358–8366.
- [33] S. Gorelsky, A. Lever, Electronic structure and spectra of ruthenium diimine complexes by density functional theory and INDO/S. Comparison of the two methods, *J. Organomet. Chem.* 635 (2001) 187–196.
- [34] T. Montanari, M. Bevilacqua, C. Resini, G. Busca, R. Pirone, G. Ruoppolo, A spectroscopic study of the nature and accessibility of protonic and cationic sites in H-and partially exchanged Cu-and Co-MFI zeolites, *J. Porous Mater.* 14 (2007) 291–297.
- [35] L. Vradman, M. Landau, D. Kantorovich, Y. Koltypin, A. Gedanken, Evaluation of metal oxide phase assembling mode inside the nanotubular pores of mesostructured silica, *Microporous Mesoporous Mater.* 79 (2005) 307–318.
- [36] M. Betiba, A. Rabie, A. Elfandy, F. Yehia, Microwave assisted synthesis of a VO_x-modified disordered mesoporous silica for ethylbenzene

dehydrogenation in presence of CO₂, *Microporous Mesoporous Mater.* 222 (2016) 44–54.

[37] G. Coudrier, T. Decamp, H. Praliaud, Comparison of copper and cobalt exchanged zeolites by ultraviolet-visible and infrared spectroscopies. Adsorption of propene and redox properties, *J. Chem. Soc. Faraday Trans. Phys. Chem. Condens. Phases* 78 (1982) 2661–2676.

[38] M.C.N.A. de Carvalho, F.B. Passos, M. Schmal, The behavior of Cu/ZSM-5 in the oxide and reduced form in the presence of NO and methanol, *Appl. Catal. A: Gen.* 193 (2000) 265–276.

[39] H. Du, C.T. Williams, A.D. Ebner, J.A. Ritter, In situ FTIR spectroscopic analysis of carbonate transformations during adsorption and desorption of CO₂ in K-promoted HTlc, *Chem. Mater.* 22 (2010) 3519–3526.

[40] Y.K. Yoo, X. Xiang, Combinatorial material preparation, *J. Phys.: Condens. Matter* 14 (2001) R49.

[41] Z.-F. Pei, V. Ponec, On the intermediates of the acetic acid reactions on oxides: an IR study, *Appl. Surf. Sci.* 103 (1996) 171–182.

[42] Z.-J. Zhao, C.-c. Chiu, J. Gong, Molecular understandings on the activation of light hydrocarbons over heterogeneous catalysts, *Chem. Sci.* 6 (2015) 4403–4425.